

Chemically Engineered Affinity Protein Drugs for Covalent Targeted Cancer Therapy

Xuelin Xia,^{*,‡} Wenhui Gao,[‡] Xiaoyuan Yang, Wei Huang, Xiao-Xia Xia,^{*} and Deyue Yan^{*}



Cite This: *J. Am. Chem. Soc.* 2025, 147, 19687–19701



Read Online

ACCESS |



Metrics & More



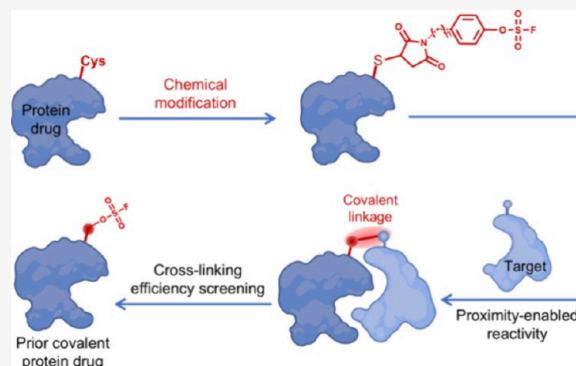
Article Recommendations



Supporting Information

ABSTRACT: Affinity proteins are multiple types of well-explored small scaffold proteins with excellent tumor targeting performance. However, due to their small size, the balance between rapid blood clearance and efficient tumor accumulation remains a challenge for their clinical application. The covalent targeting mode, endowing the affinity proteins with an irreversible binding ability to their receptor and then decoupling the pharmacodynamic effect from pharmacokinetics, may provide a promising solution for clinical applications of affinity proteins. Herein, we develop a chemical modification strategy to construct covalently targeted affinity protein drugs. Through the chemical attachment with a sulfur(VI) fluoride exchange (SuFEx) chemistry-based maleimide-substituted aryl fluorosulfate (MFS) linker, the engineered affinity protein acquires the capacity to covalently link with its targeting receptor.

As a proof of concept, the MFS linker modified affibody-protein drug elicited over 72% covalent binding to the target human epidermal growth factor receptor 2 (HER2) and 185% higher cell uptake than that of the noncovalent control *in vitro*. In mice, the tumor retention capacity of the covalent affibody-protein drug was 2.01 times greater than that of the control group, ultimately resulting in nearly complete inhibition of tumor growth. Similar enhanced therapeutic efficacy was also obtained in another MFS linker-armed monobody-protein drug targeting the epidermal growth factor receptor (EGFR). In brief, this facile chemical modification strategy provides a general platform for preparing covalently targeted affinity protein drugs, potentially accelerating the application of protein therapeutics in diverse diseases.



INTRODUCTION

Affinity proteins (e.g., affibodies, monobodies, anticalins, and nanobodies) represent diverse classes of scaffold proteins. They are considered as viable alternatives to monoclonal antibodies owing to their unique properties, such as small size, high target affinity, flexible structure, and ready availability.^{1–3} The small size of affinity proteins is beneficial for their rapid targeting and tissue penetration but simultaneously leads to the rapid elimination of them by kidneys, resulting in limited tumor retention, which has become the Achilles' heel of them. Thus, numerous affinity protein drugs were explored for cancer therapy over the past decade; however, few actually entered clinical applications.^{4–7}

In general, a successful targeted drug typically requires the following characteristics: excellent tumor targeting, enough tumor retention, and rapid residue metabolism. Only then can a sufficient amount of drug molecules be delivered to the tumor tissue with the least impact on normal organs.^{8,9} Benefiting from the outstanding targeting ability, traditional affinity protein drugs usually can rapidly target tumor cells. However, due to the reversible interaction of the affinity protein with its target, the tumor retention of these drugs is often inadequate, which restricts their efficacy in cancer therapy.¹ A covalent drug can irreversibly bind with its target

by forming a covalent linkage between both, endowing it with a strong and long-lasting action time.^{10–12} Thus, we surmised that the tumor uptake and retention of affinity protein drugs might be enhanced effectively by endowing them with a covalent binding ability. It can be imagined that if the affinity protein drugs could bind irreversibly with their cancer targets, then a promising drug delivery pattern integrating excellent tumor targeting, enough tumor retention, and rapid residue metabolism could be anticipated.

Sulfur fluoride exchange (SuFEx), an emerging type of click chemistry reaction, demonstrates great potential for the covalent binding of molecules in living organisms.^{13–15} The reported proximity-enabled reactivity of them can endow themselves with high stability and bioorthogonality prior to reacting with their targets. Several SuFEx latent warheads are investigated to cross-link protein/small-molecule inhibitors,^{8,16}

Received: February 5, 2025

Revised: May 15, 2025

Accepted: May 19, 2025

Published: May 30, 2025



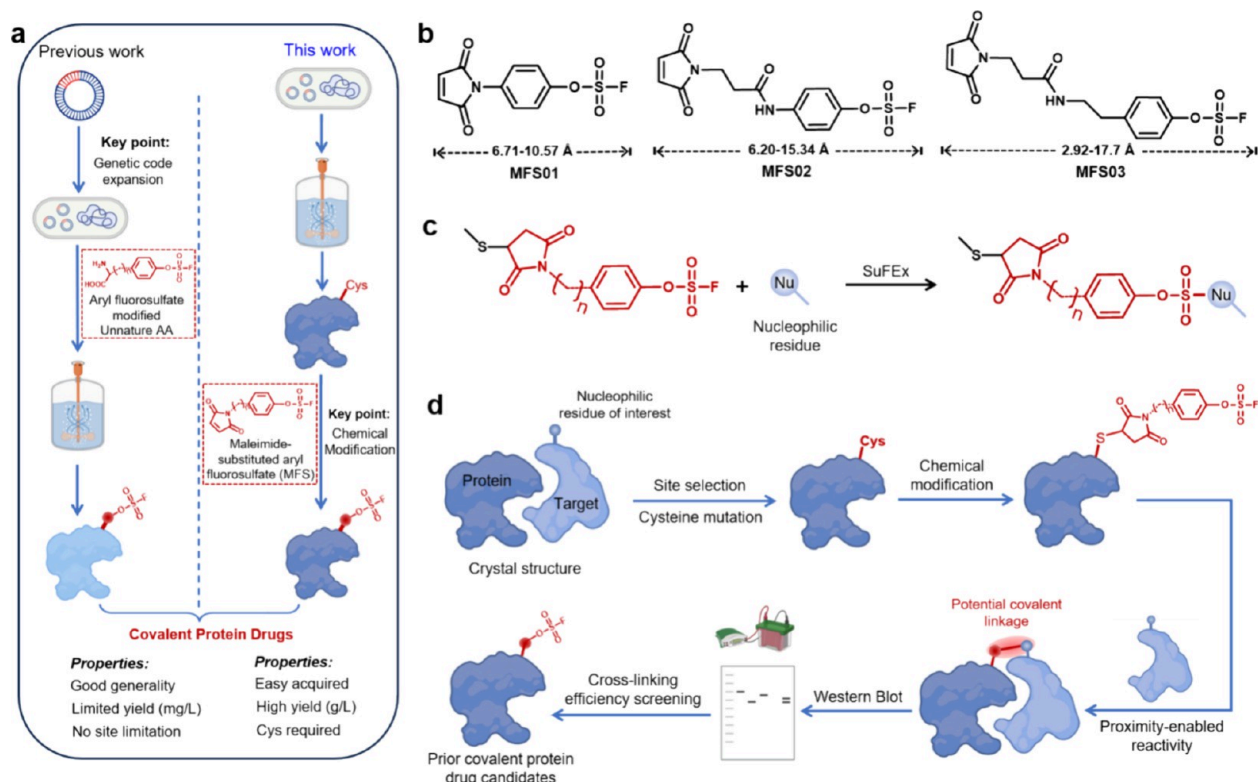


Figure 1. Illustration of the chemical modification strategy to construct covalent targeted affinity protein drugs. (a) Overview of the previous genetic code expansion method and current chemical modification strategy for preparing covalent protein drugs. (b) Detailed chemical structure of MFS linkers. The dashed lines show the minimum and maximum distances between the starting carbon atom and the ending fluorine atom calculated by GROMACS. (c) The MFS linker at the affinity protein drug reacts with a proximal nucleophilic residue of target protein via click chemistry SuFEx. (d) Overall procedure to develop a covalent affinity protein drug.

protein/protein,^{17–19} protein/carbohydrate,²⁰ and protein/nucleic acids.²¹ Currently, SuFEx latent warheads are mainly encapsulated in unnatural amino acids (Uaas) and subsequently site-specifically incorporate into protein drugs via genetic code expansion technology.^{22–24} This technical approach is rather ingenious in introducing Uaas into proteins. However, the yield of target proteins is restricted (less than 10 mg/L) due to the recognition limitations of Uaas by native cellular systems; thereby, it is still a challenge to achieve large-scale preparation (Figure 1a left).¹⁷ Therefore, it is highly desirable to explore a universal high-yield approach to prepare protein drugs containing SuFEx latent warheads.

Herein, we explore a novel synthetic route by the direct modification of proteins with SuFEx latent warheads without needing for genetic code expansion; meanwhile, proteins used here can be produced in large quantities through fermentation techniques (Figure 1a). As a proof of concept, several maleimide-substituted aryl fluorosulfate (MFS) linkers were synthesized (Figure 1b) and subsequently attached at the selected amino acid site of an affinity protein in accordance with its relevant crystal structure data. The introduction of the MFS linker endowed these affinity protein drugs with great potential of covalently binding with their target through proximity-enabled reactivity (Figure 1c); thus, we consider this to be a rather efficient approach to transform classical protein drugs into a covalent pattern.

We selected two common affinity proteins, namely, the affibody (Z_{HER2:342}) and monobody (Adnectin), as the targeting moiety to construct protein conjugates with PE24 (*Pseudomonas aeruginosa* exotoxin, a promising anticancer

agent).^{25–27} The detailed design process is depicted in Figure 1d. First, crystal structure data of the protein/target complex were analyzed, and further cysteine mutation was introduced at the appropriate amino acid sites of the affinity protein. Second, one of various SuFEx-engineered MFS linkers with different lengths was attached to the cysteine residue through thiol chemistry to produce a covalent drug candidate. Third, the obtained drug candidate was incubated with its targeting receptor and the cross-linking efficiency was analyzed via Western blotting. Finally, the covalent affinity protein drug with the highest cross-linking efficiency was screened out as the preferred drug and utilized for further trials.

RESULTS AND DISCUSSION

Synthesis and Characterization of MFS Linkers.

According to previous reports, the distance between the F atom and the reactive residues is crucial for the occurrence of proximity-enabled SuFEx reaction.^{28,29} To meet the spatial requirement of proximity-enabled reactivity and enhance the cross-linking efficiency between the protein drug and its target, three maleimide-substituted aryl fluorosulfate (MFS_n, *n* = 01, 02, and 03) linkers of various lengths (6.71–10.57, 6.20–15.34, and 2.92–17.7 Å, respectively) were synthesized for subsequent comparative screening (Figure 1b and Figures S1 and S2). In detail, the corresponding phenol substrate was initially reacted with (4-acetamidophenyl)(fluorosulfonyl) aminosulfonyl fluoride (AISF) to generate the intermediate sulfonyl fluoride compound³⁰ and subsequently amidated with 3-maleimide propionic acid as needed to obtain the target product. The structure and molecular weight of these products

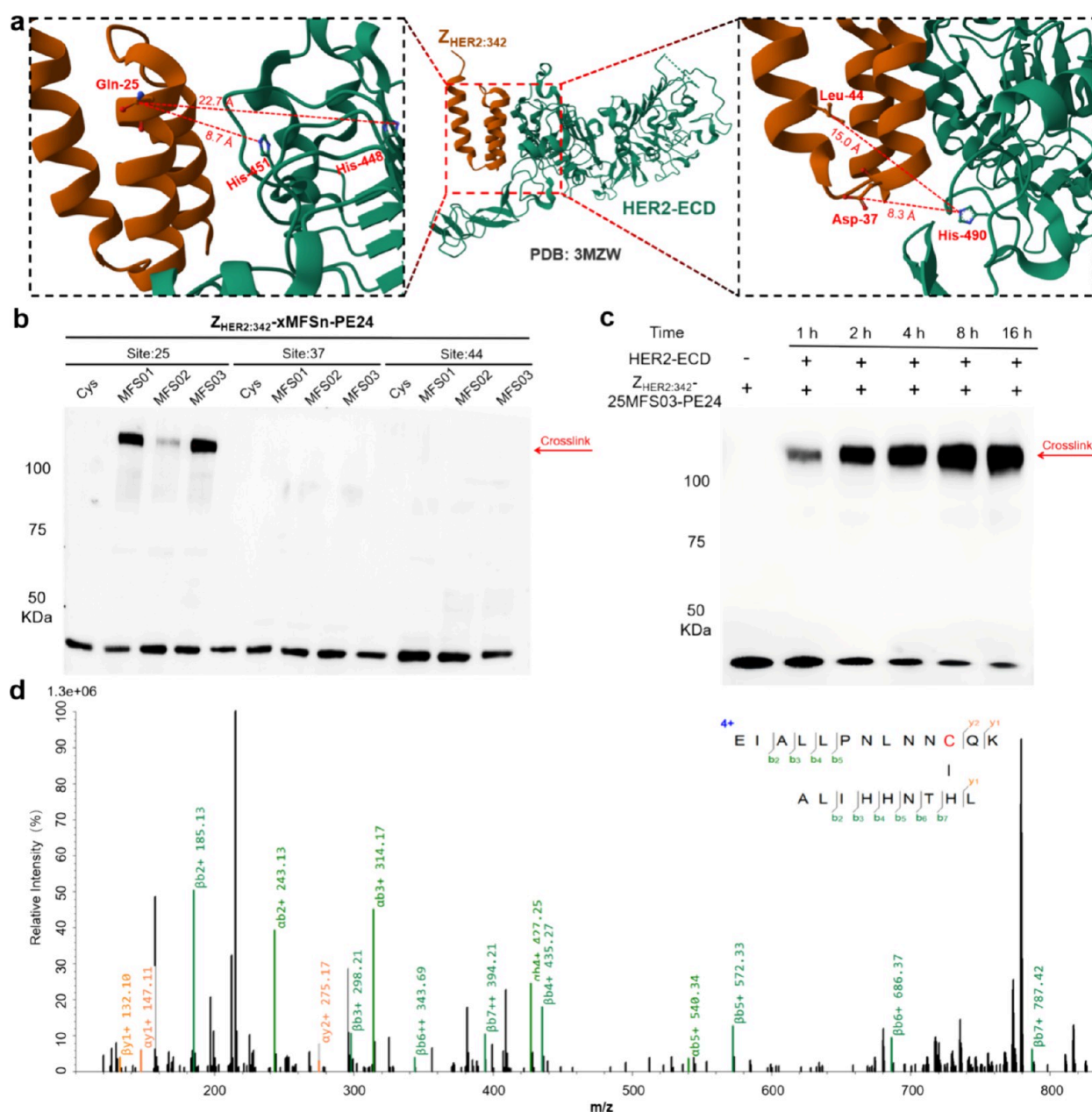


Figure 2. Covalently cross-linked Z_{HER2:342}-xMFSn-PE24 with its targeting receptor HER2 irreversibly *in vitro*. (a) Crystal structure of the Z_{HER2:342}/HER2-ECD complex (PDB 3MZW), showing the MFS linker incorporation site (Asp37, Leu44, and Gln25) in Z_{HER2:342} and the potential target residue (His448, His451, and His490) in HER2. (b) Western blot analysis of various Z_{HER2:342}-xMFSn-PE24 conjugates binding to HER2 *in vitro*. Red arrows indicate the covalent product of Z_{HER2:342}-xMFSn-PE24/HER2. (c) Time-course studies of the cross-linking efficiency between Z_{HER2:342}-25MFS03-PE24 and HER2, as verified by Western blotting. (d) Tandem mass spectrum of the Z_{HER2:342}-25MFS03-PE24/HER2 complex indicated that MFS03 at site 25 on Z_{HER2:342}-25MFS03-PE24 cross-linked with His451 of HER2. Data are presented as means \pm SD from three (b–d) independent experiments.

were verified by nuclear magnetic resonance (NMR) and liquid chromatography–mass spectrometry (LC-MS), and the results presented in [Data S1](#) clearly demonstrated that the MFS linkers were successfully synthesized.

Construction of Covalent Targeted Affinity Protein Drugs. Two series of affinity protein drugs were initially expressed through *Escherichia coli* (*E. coli*) fermentation. The structural composition design and amino acid sequence are presented in [Figures S3 and S4](#). Subsequently, after purification, the obtained protein drugs were attached with different MFS linkers to prepare their corresponding covalent

patterns ([Figure S5](#)). In this manner, multiple covalent affinity protein drugs were rapidly prepared for subsequent screening.

In detail, according to crystal structure data of the Z_{HER2:342}/HER2 complex (PDB 3MZW) in [Figure 2a](#), the distances from Gln25, Asp37, and Leu44 of Z_{HER2:342} to His448, His451, or His490 of HER2-ECD are around 8.3–22.7 Å, which can be effectively covered by the length of the MFS linker. Based on these, three affinity protein drugs, namely, Z_{HER2:342}-x-Cys-PE24 (where *x* represents the position 25, 37, or 44), were prepared by mutating specific sites in the original Z_{HER2:342} sequence to cysteine. These protein drugs were first expressed in *E. coli* and purified using the Ni-nitrilotriacetyl agarose

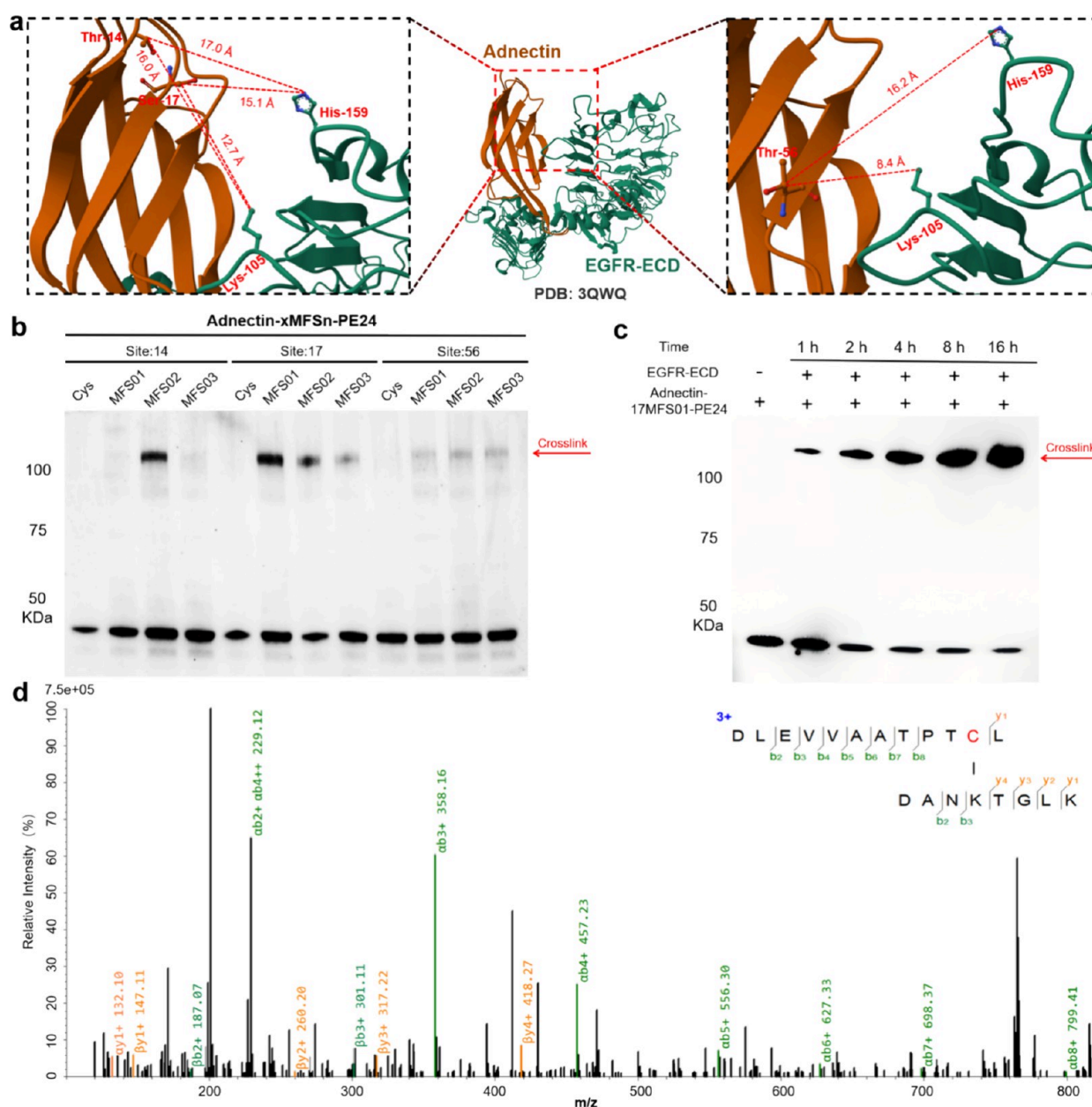


Figure 3. Adnectin- x MFS n -PE24 covalently cross-links with its EGFR target irreversibly *in vitro*. (a) Crystal structure of the Adnectin/EGFR-ECD complex (PDB 3QWQ), showing the MFS linker incorporation site (Thr14, Ser17, and Thr56) in Adnectin and the potential target residues (Lys105 and His159) in EGFR. (b) Western blot analysis of various Adnectin- x MFS n -PE24 conjugates binding to EGFR *in vitro*. Red arrows indicate the covalent product of Adnectin- x MFS n -PE24/EGFR. (c) Time-course studies of the cross-linking efficiency between Adnectin-17MFS01-PE24 and EGFR, as verified by Western blotting. (d) Tandem mass spectrum of the Adnectin-17MFS01-PE24/EGFR complex indicated that MFS01 at site 17 on Adnectin-17MFS01-PE24 cross-linked with Lys105 of EGFR. Data are presented as means \pm SD from three (b–d) independent experiments.

column. Then, they were conjugated with three MFS linkers to obtain aryl fluorosulfate-modified $Z_{\text{HER2:342}}-x\text{MFS}_n\text{-PE24}$ conjugates (where n represents the serial number of MFS linkers 01, 02, and 03). Finally, the molecular weight of each product was confirmed by matrix-assisted laser desorption/ionization time-of-flight mass spectrometry (MALDI-TOF-MS), and the results (Data S2) exhibited the molecular weights of $Z_{\text{HER2:342}}-x\text{Cys-PE24}$ and the corresponding $Z_{\text{HER2:342}}-x\text{MFS}_n\text{-PE24}$, which precisely matched their theoretical mass, thereby confirming the successful preparation of nine types of $Z_{\text{HER2:342}}-x\text{MFS}_n\text{-PE24}$.

Meanwhile, referring to crystal structure data of the Adnectin/EGFR complex (PDB 3QWQ), we initially identified Thr14, Ser17, and Thr56 of Adnectin as candidate cysteine mutation sites, based on their potential reactivity with Lys105 or His159 of EGFR-ECD. The distances from these amino acids of Adnectin to Lys105 or His159 of EGFR-ECD were approximately 8.4–17.0 Å (Figure 3a), which could also be covered by the MFS linkers. Based on these data, three Adnectin- x Cys-PE24 protein drugs (where x represents positions 14, 17, and 56) were designed and prepared and ultimately conjugated with different MFS linkers to obtain Adnectin- x MFS n -PE24 conjugates. The molecular weight of

each product was detected and is presented in [Data S3](#), which was in excellent agreement with its theoretical value, confirming the successful preparation of nine types of Adnectin-*x*MFS*n*-PE24.

Covalent Affinity Protein Drugs Bind to Their Targets Irreversibly. To verify whether the attachment of the MFS linker could trigger the proximity-enabled SuFEx reaction with the adjacent nucleophilic residues, we further analyzed the covalent cross-linking efficiency and the cross-linking site of the prepared covalent drugs containing different MFS linkers with their targets and screened out the optimum site-linker combination. As shown in [Figure 2b](#), the introduction of these MFS linkers at site 25 of $Z_{\text{HER2:342}}\text{-}x\text{MFS}n\text{-PE24}$ induced noticeable bands at 150 kDa after incubation with HER2-ECD, which corresponded to the covalent-linking products of $Z_{\text{HER2:342}}\text{-}25\text{MFS}n\text{-PE24}$ (with a molecular weight of approximately 36.8 kDa) and HER2-ECD (with a molecular weight of approximately 110 kDa), evidently demonstrating that the covalent cross-linking occurred between MFS and its proximal nucleophilic residues. Meanwhile, no obvious cross-linking was observed when the MFS linker was introduced at positions 37 and 44, suggesting that the length or the direction of the MFS linker at these sites might not be suitable for triggering the proximity-enabled reactivity with the neighboring nucleophilic residues.

In order to further determine the location where the cross-linking occurred between the MFS linker at site 25 of $Z_{\text{HER2:342}}$ and the nucleophilic residues of HER2-ECD, the cross-linked bands were collected, enzymatically digested, and then analyzed by tandem mass spectrometry.^{31,32} As shown in [Figure 2d](#), a series of *b* and *y* ions of the cross-linked peptide were extracted, which evidently demonstrated that MFS03 of $Z_{\text{HER2:342}}\text{-}25\text{MFS03-PE24}$ reacted with His451 of HER2-ECD. Meanwhile, we further identified the cross-linked peptide in the $Z_{\text{HER2:342}}\text{-}25\text{MFS01-PE24}$ and $Z_{\text{HER2:342}}\text{-}25\text{MFS02-PE24}$ groups, and the results also explicitly indicated that both MFS01 and MFS02 at site 25 reacted with His451 of HER2-ECD ([Figures S6 and S7](#)). Among these, MFS01 (6.71–10.57 Å) exhibited a similar cross-link efficiency to that of MFS03 (2.92–17.7 Å), possibly attributed to their flexible straight-chain structure. However, the coupling efficiency of MFS02 (6.20–15.34 Å) is significantly lower; we speculated that the curved molecular structure of MFS02 ([Figure S2](#)) might not be conducive to the binding of the F atom and histidine. Additionally, no other residues of HER2 were found to react with all three MFS linkers, indicating that $Z_{\text{HER2:342}}\text{-}25\text{MFS}n\text{-PE24}$ covalently targeted HER2 at His451 in a highly specific manner. Above all, the introduction of MFS03 at site 25 resulted in the highest cross-linking efficiency with HER2-ECD, and thus, $Z_{\text{HER2:342}}\text{-}25\text{MFS03-PE24}$ was selected for subsequent experiments.

To further evaluate the kinetics of covalent complex formation, $Z_{\text{HER2:342}}\text{-}25\text{MFS03-PE24}$ was incubated with HER2-ECD for various time periods and analyzed by Western blotting. As depicted in [Figure 2c](#) and [Figure S8](#), the cross-linking band could be immediately observed after 1 h of incubation and the covalent cross-linking products gradually accumulated as the incubation time prolonged. After 16 h of incubation, prominent cross-linked complexes were formed with a yield of $72.08 \pm 1.22\%$, which was consistent with the results of SDS-PAGE as shown in [Figure S9](#). All of these data clearly indicated that $Z_{\text{HER2:342}}\text{-}25\text{MFS03-PE24}$ rapidly and efficiently cross-linked HER2-ECD *in vitro*.

Meanwhile, we also explored the cross-linking status between Adnectin-*x*MFS*n*-PE24 and EGFR-ECD. As shown in [Figure 3b](#), the introduction of MFS linkers at sites 14, 17, and 56 of Adnectin-*x*MFS*n*-PE24 could induce observable cross-linking bands at 150 kDa after incubation with EGFR-ECD, which precisely matched the covalent-linking products of Adnectin-*x*MFS*n*-PE24 (with a molecular weight of approximately 41.7 kDa) and EGFR-ECD (with a molecular weight of approximately 110 kDa). Specifically, for site 14, only the introduction of MFS02 resulted in a notable band at 150 kDa; for site 17, the introduction of MFS01 and MFS02 both could lead to noticeable bands, and among these, Adnectin-17MFS01-PE24 exhibited the highest cross-linking efficacy; finally, for site 56, the introduction of the MFS linkers led to negligible bands, which might be attributed to the fact that the molecule orientation at site 56 is unfavorable for MFS to approach its adjacent nucleophilic residues.

To further validate the chemical cross-linking site between Adnectin-*x*MFS*n*-PE24 and EGFR-ECD, we also subjected the protein bands to tandem MS analysis. As shown in [Figure 3d](#), robust signals corresponding to the covalently linked peptides were identified, suggesting that the incorporated MFS01 (6.71–10.57 Å) at site 17 cross-linked exclusively with Lys105 of EGFR-ECD. Meanwhile, the tandem MS result presented in [Figure S10](#) also indicated that MFS02 (6.20–15.34 Å) at site 14 cross-linked with Lys105 specially. Surprisingly, as shown in the identification result in [Figure S11](#), MFS02 introduced at site 17 could react simultaneously with Lys105 and His159 of EGFR-ECD; however, despite the availability of dual targets for reaction, its overall coupling efficiency is still not high, which might be attributed to the improper molecular angle of MFS02. In addition, no other residues of EGFR were found to react with these MFS linkers. Based on the above results, we thus selected the most efficient Adnectin-17MFS01-PE24 for subsequent experiments.

Then, we conducted a further investigation on the time-dependent cross-linking of Adnectin-17MFS01-PE24 with EGFR-ECD. As shown in [Figure 3c](#) and [Figure S12](#), the cross-linking band was detectable within 1 h of incubation, and eventually, approximately $70.07 \pm 3.01\%$ of the cross-linked complexes were formed within 16 h of incubation. These results were also verified by SDS-PAGE data in [Figure S13](#), further confirming the extraordinary cross-linking efficiency of Adnectin-17MFS01-PE24 with EGFR-ECD.

In addition, we also examined the effect of cysteine mutation and covalent modification on the binding ability of affinity proteins to their target by biolayer interferometry.³³ On the basis of affinity constants presented in [Figure S14](#), the equilibrium dissociation constants (K_D) of $Z_{\text{HER2:342}}\text{-}25\text{MFS03-PE24}$ and Adnectin-PE24 were about 2.37×10^{-9} and 1.64×10^{-9} M, respectively. After the cysteine mutation, the K_D of $Z_{\text{HER2:342}}\text{-}25\text{Cys-PE24}$ and Adnectin-17Cys-PE24 changed to 6.04×10^{-9} and 3.03×10^{-9} M, respectively. The slight decrease may be attributed to the effect of mutating a residue to Cys in the binding pocket. Furthermore, after the attachment of the MFS linker, the K_D of the resulting $Z_{\text{HER2:342}}\text{-}25\text{MFS03-PE24}$ and Adnectin-17MFS01-PE24 reached approximately 2.10×10^{-9} and 1.44×10^{-9} M, respectively, representing 2.85-fold and 2.10-fold lower than those of $Z_{\text{HER2:342}}\text{-}25\text{Cys-PE24}$ and Adnectin-17Cys-PE24. All in all, both $Z_{\text{HER2:342}}\text{-}25\text{MFS03-PE24}$ and Adnectin-17MFS01-PE24 demonstrated an enhanced affinity ability compared to their noncovalent patterns and outperformed the original

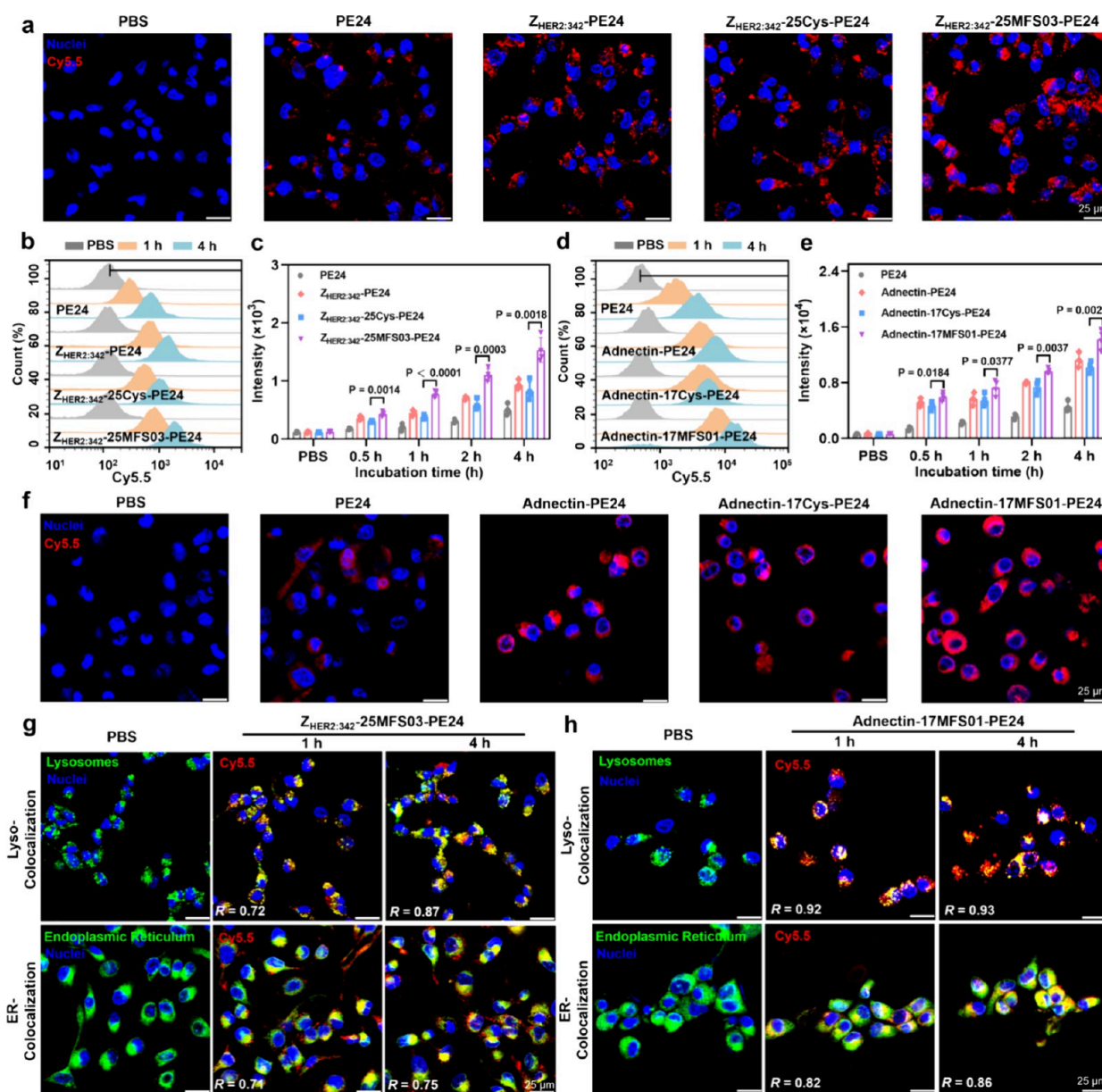


Figure 4. Increased cellular uptake of covalent targeted affinity protein drugs. (a) Integrated CLSM images of SKOV-3 cells after 4 h of incubation of PE24, $Z_{HER2:342}$ -PE24, $Z_{HER2:342}$ -25Cys-PE24, and $Z_{HER2:342}$ -25MFS03-PE24 (all the drugs were labeled with Cy5.5). The detailed single stained images are exhibited in Figure S15. Flow cytometry results (b) and corresponding quantitative analysis (c) of SKOV-3 cells treated with various drugs at different time points. The detailed results at different time points are included in Figure S16. Flow cytometry results (d) and corresponding quantitative analysis (e) of A-431 cells treated with various drugs at different time points. The detailed results at different time points are included in Figure S20. (f) Integrated CLSM images of A-431 cells after 4 h of incubation of PE24, Adnectin-PE24, Adnectin-17Cys-PE24, and Adnectin-17MFS01-PE24 (all the drugs were labeled with Cy5.5). The detailed single stained images are exhibited in Figure S19. (g) Integrated CLSM images of the lysosome (Lyso) and endoplasmic reticulum (ER) colocalization assay in SKOV-3 cells treated with Cy5.5-labeled $Z_{HER2:342}$ -25MFS03-PE24 for specified time intervals. R represents the Pearson correlation coefficient. The detailed single stained images are shown in Figure S18. (h) CLSM images of the Lyso and ER colocalization assay in A-431 cells treated with Cy5.5-labeled Adnectin-17MFS01-PE24 for specified time intervals. The detailed single stained images are shown in Figure S22. Scale bar: 25 μ m. P values are determined with two-tailed unpaired Student's t test. Data are presented as means \pm SD from three (a–e) independent experiments.

$Z_{HER2:342}$ -PE24 and Adnectin-PE24. This significant improvement can be attributed to the irreversible binding of affinity proteins to their targets, and even the effect of mutation is compensated by enhanced activity resulting from covalent binding to the target.

Covalent Binding Enhances the Cellular Uptake of Affinity Protein Drugs. Covalent binding may effectively enhance the cellular uptake and retention of affinity protein drugs.^{34,35} Herein, various Cy5.5-labeled affinity protein drugs

were first prepared and employed to investigate the cellular uptake behaviors and internalization processes by confocal laser scanning microscopy (CLSM) and flow cytometry. As shown in Figure 4a,b and Figures S15 and S16, a remarkable cellular uptake of $Z_{HER2:342}$ -25MFS03-PE24 was observed within SKOV-3 cells (human ovarian adenocarcinoma cells with a high HER2 expression), and the uptake efficiency was significantly higher than that of $Z_{HER2:342}$ -PE24 and $Z_{HER2:342}$ -25Cys-PE24 groups after 4 h of incubation. The quantitative

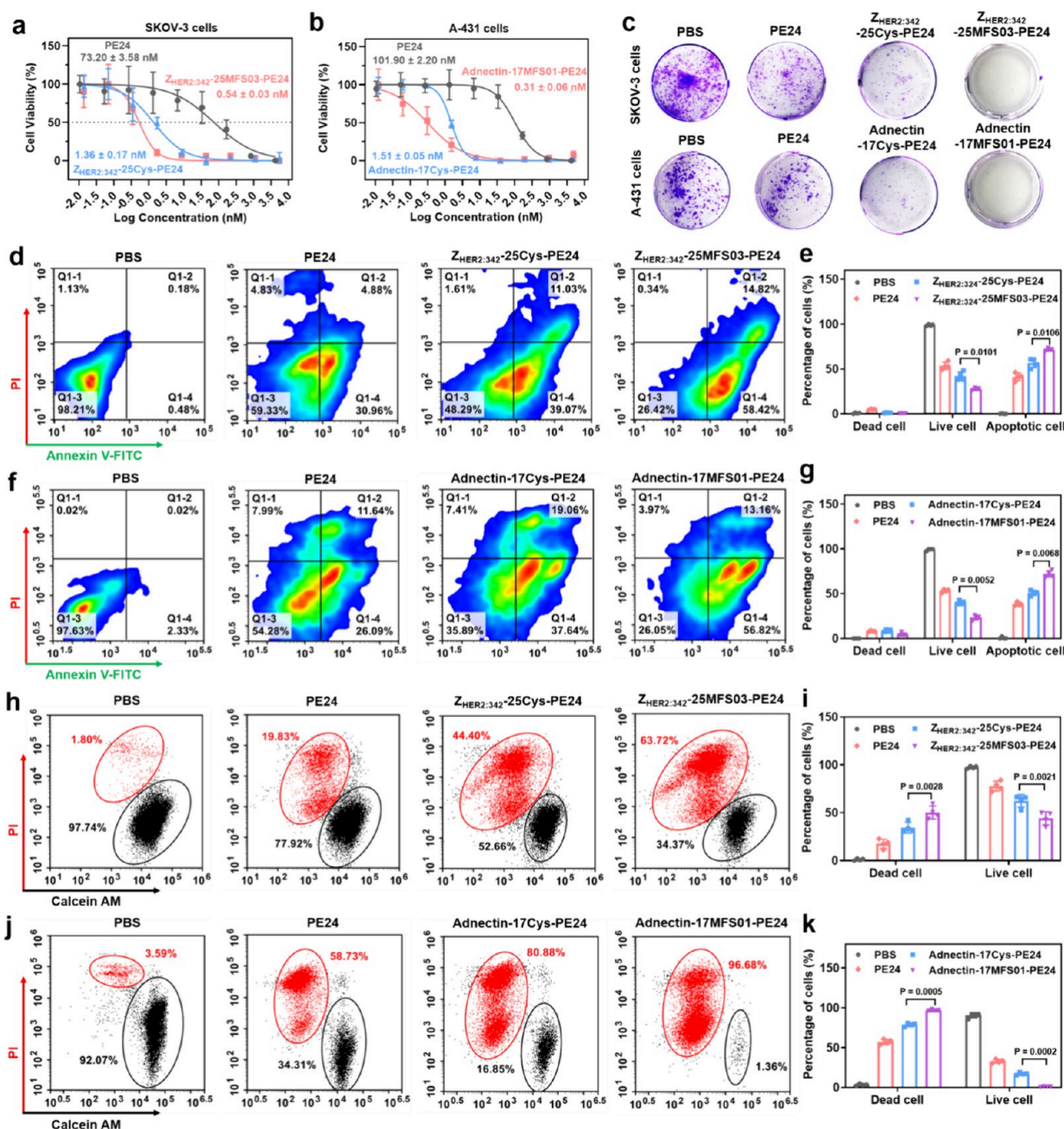


Figure 5. Enhanced cytotoxicity of covalent targeted affinity protein drugs. Relative cell viabilities of SKOV-3 (a) and A-431 (b) cells after 48 h of incubation with corresponding drugs. (c) Colony formation images of SKOV-3 and A-431 cells after different treatments. Apoptosis assay of SKOV-3 cells (d, e) and A-431 cells (f, g) treated with related drugs, followed by the measurement of flow cytometry and corresponding quantitative analysis. Flow cytometry images and the corresponding quantitative data of the Calcein-AM/PI containing assay for SKOV-3 cells (h, i) and A-431 cells (j, k) after different treatments. *P* values are determined with two-tailed unpaired Student's *t* test. Data are presented as means ± SD from six (a, b), three (c), or four (d, k) independent experiments.

analysis of flow cytometry in Figure 4c verified the higher time-dependent uptake trend for Z_{HER2:342}-25MFS03-PE24, and the accumulation of Z_{HER2:342}-25MFS03-PE24 in cancer cells was approximately 1.85-fold greater than that of noncovalent Z_{HER2:342}-25Cys-PE24 after 4 h of incubation. These data confirmed that the covalent binding could enhance the cellular uptake of affinity protein drugs indeed.

The cellular internalization mechanism of Z_{HER2:342}-25MFS03-PE24 was further explored through a competitive inhibition assay.^{5,36} SKOV-3 cells were preincubated with free Z_{HER2:342} for 1 h, followed by coinubation with Cy5.5-labeled

Z_{HER2:342}-25MFS03-PE24 for an additional 4 h. The flow cytometry results in Figure S17 demonstrated that the preincubation with free Z_{HER2:342} obvious hindered the internalization of Z_{HER2:342}-25MFS03-PE24 by SKOV-3 cells, confirming that Z_{HER2:342}-25MFS03-PE24 was internalized by cells via HER2-mediated endocytosis. Furthermore, along with the cellular internalization, the PE24 toxin was supposed to be released through the cleavage of the designed enzyme cleavage site (RHRQPRGWEL) by fulin protease in the acidic lysosome environment, and subsequently, the released PE24 activity domain was transported to the endoplasmic reticulum

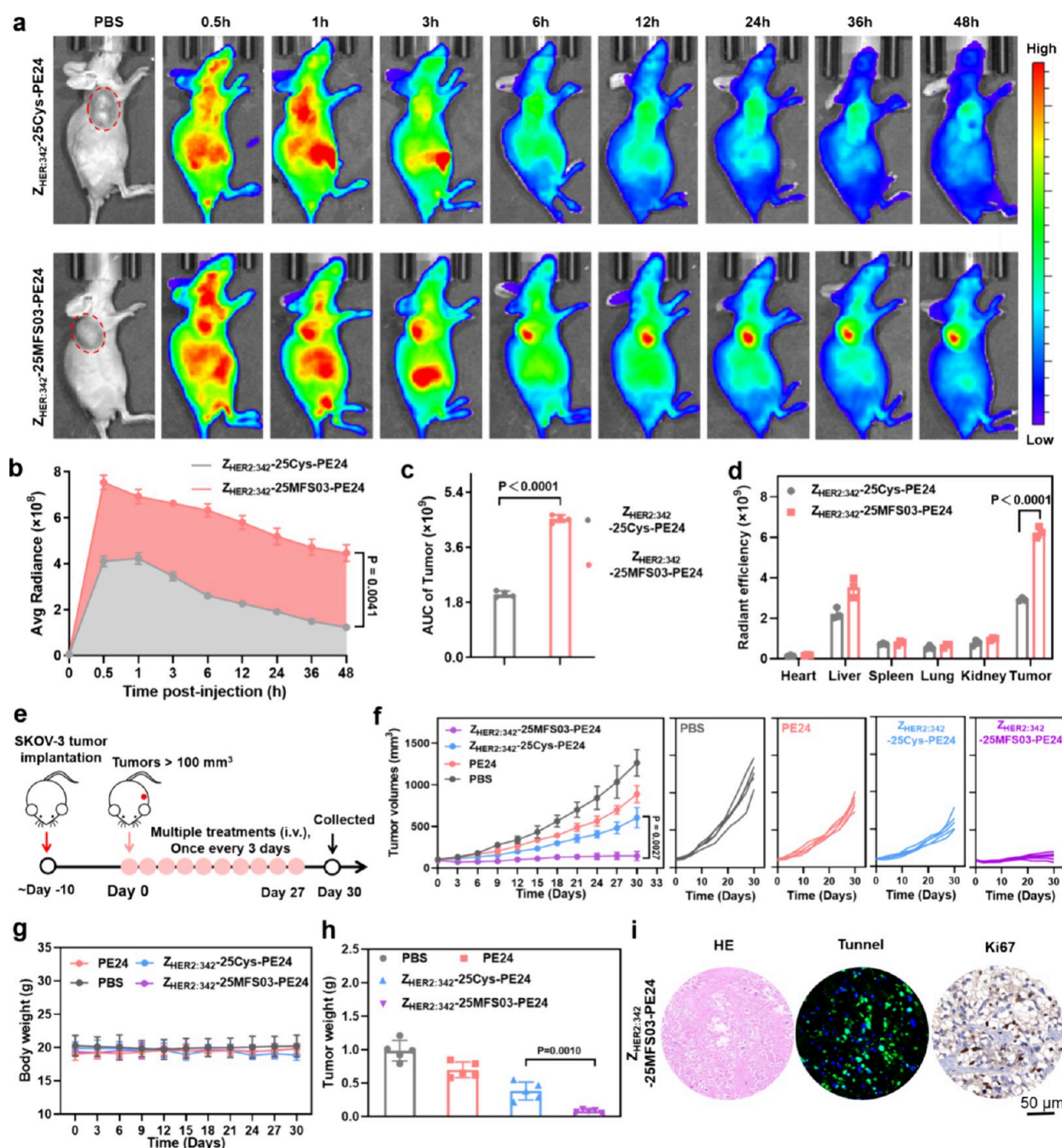


Figure 6. Improved tumor uptake and enhanced antitumor efficacy of $Z_{HER2:342-25MFS03-PE24}$ in the HER2 overexpressed tumor model. (a) *In vivo* fluorescence imaging of the SKOV-3 tumor model treated with Cy5.5-labeled $Z_{HER2:342-25Cys-PE24}$ and Cy5.5-labeled $Z_{HER2:342-25MFS03-PE24}$. The red dashed circle indicates the tumor site. (b) Time-fluorescence intensity curves of tumor sites within the 48 h period after administration. (c) Integrated area under the curve (AUC) of different groups. (d) Quantitative analysis of tissue distribution in mice of different groups after injection of 48 h. (e) Schematic diagram of the antitumor experiment. (f) Tumor growth curves of each group with different treatments. (g) Body weight changes of the mice during the treatment. (h) Average weight of collected tumors at the end of experiment. (i) Histological and immunohistochemical analysis of the residual tumor in the $Z_{HER2:342-25MFS03-PE24}$ group (the related results of other groups are exhibited in Figure S24). *P* values are determined with two-tailed unpaired Student's *t* test. Data are presented as means \pm SD from three (d, i), four (a–c), or five (f–h) independent experiments.

to exert its activity.^{27,37,38} To verify this pathway, the lysosome (Lyso) and endoplasmic reticulum (ER) colocalization assay was conducted on SKOV-3 cells using Cy5.5-labeled $Z_{HER2:342-25MFS03-PE24}$. As shown in Figure 4g and Figure S18, the CLSM images revealed significant fluorescence overlap between Cy5.5 and Lyso-Tracker/ER-Tracker after 1 h of coinubation, and the overlap efficiency gradually increased

within 4 h, with Pearson correlation coefficients of approximately 0.87 and 0.75, respectively, suggesting the efficient enrichment of $Z_{HER2:342-25MFS03-PE24}$ in the lysosome and endoplasmic reticulum. All of the above results collectively confirmed that $Z_{HER2:342-25MFS03-PE24}$ could be effectively internalized by cancer cells and released PE24, thereby exerting its antitumor activity.

In addition, we investigated the cellular uptake behavior of Adnectin-17MFS01-PE24 in A-431 cells (human epidermal cancer cells with a high EGFR expression), as shown in Figure 4d,f and Figures S19 and S20. Compared with the Adnectin-PE24 and Adnectin-17Cys-PE24 groups, the incubation of the covalent Adnectin-17MFS01-PE24 exhibited a significantly faster uptake efficiency within 4 h incubation. The quantitative analysis of flow cytometry in Figure 4e demonstrated that the cell accumulation of Adnectin-17MFS01-PE24 was about 1.39-fold higher than that of Adnectin-17Cys-PE24 after incubation for 4 h. The cellular internalization mechanism of Adnectin-17MFS01-PE24 was also explored, and the flow cytometry results in Figure S21 indicated that the preincubation with free Adnectin blocked the internalization of Adnectin-17MFS01-PE24 by A-431 cells, confirming that Adnectin-17MFS01-PE24 was internalized by cells through EGFR-mediated endocytosis. Furthermore, the Lyso/ER colocalization assay was performed on A-431 cells with Cy5.5-labeled Adnectin-17MFS01-PE24. As shown in Figure 4h and Figure S22, the CLSM images revealed notable fluorescence overlap between Cy5.5 and Lyso-Tracker/ER-Tracker after 1 h of incubation, and the overlap efficiency gradually rose within 4 h, with Pearson correlation coefficients of approximately 0.93 and 0.86. Overall, these results confirmed the enhanced cellular uptake capacity of affinity protein drugs upon the introduction of covalent binding and verified a possible cellular internalization mechanism.

Covalent Binding Enhances the Cytotoxicity of Affinity Protein Drugs. Typically, an enhanced cellular uptake behavior could potentially result in increased drug cytotoxicity for cancer cells. Thus, we inferred that covalent affinity protein drugs were likely to demonstrate the greater cytotoxicity against cancer cells compared to their noncovalent counterparts. Here, a series of assays were performed to evaluate the effect of introducing the covalent binding ability into affinity protein drugs on their cytotoxicity. First, the antiproliferative activity of covalent affinity protein drugs was assessed by the CCK-8 assay. As shown in Figure 5a,b and Figure S23, the Cys-mutated protein drugs $Z_{\text{HER2:342}}\text{-25Cys-PE24}$ (IC_{50} values of 1.36 ± 0.17 nM) and Adnectin-17Cys-PE24 (IC_{50} values of 1.51 ± 0.05 nM) exhibited similar cytotoxicity against both SKOV-3 cells and A-431 cells, relative to their nonmutated counterparts $Z_{\text{HER2:342}}\text{-PE24}$ and Adnectin-PE24 (IC_{50} values were 1.08 ± 0.33 and 0.79 ± 0.10 nM, respectively), demonstrating the limited effect of Cys mutation in the binding pocket to the related cytotoxicity. Moreover, the covalent $Z_{\text{HER2:342}}\text{-25MFS03-PE24}$ exhibited the remarkable cytotoxicity against SKOV-3 cells with an IC_{50} value of 0.54 ± 0.03 nM, which was 2.5-fold lower than that of the noncovalent $Z_{\text{HER2:342}}\text{-25Cys-PE24}$. Meanwhile, Adnectin-17MFS01-PE24 also displayed notable cytotoxicity against A-431 cells, with an IC_{50} value of 0.31 ± 0.06 nM, which was 4.9-fold lower than that of the noncovalent Adnectin-17Cys-PE24. Additionally, the antiproliferative effects of covalent affinity protein drugs were further explored in related cancer cells through the colony formation assay. As shown in Figure 5c, the covalent $Z_{\text{HER2:342}}\text{-25MFS03-PE24}$ and Adnectin-17MFS01-PE24 exhibited more pronounced inhibition of clonogenicity in SKOV-3 or A-431 cells compared to their noncovalent counterparts. These results confirmed the enhanced cytotoxicity of affinity protein drugs with covalent binding modification.

Subsequently, apoptosis analysis was further conducted by employing an Annexin V-FITC/PI staining assay. As shown in Figure 5d, the highest apoptotic rate of SKOV-3 cells was observed in the $Z_{\text{HER2:342}}\text{-25MFS03-PE24}$ group (73.58%), in contrast to those groups of the PBS (1.79%), PE24 (40.67%), and $Z_{\text{HER2:342}}\text{-25Cys-PE24}$ (51.71%). Moreover, the quantitative analysis results in Figure 5e indicated that the apoptotic cell ratio of $Z_{\text{HER2:342}}\text{-25MFS03-PE24}$ was 1.27 times higher than that of $Z_{\text{HER2:342}}\text{-25Cys-PE24}$. Additionally, similar apoptosis outcomes were also observed in A-431 cells treated with Adnectin-17MFS01-PE24 (Figure 5f,g), where the cell apoptotic rate reached up to 73.95%, which was 1.41 times higher than that of cells treated with Adnectin-17Cys-PE24.

Furthermore, the Live/Dead assay was carried out by flow cytometry through the Calcein-AM/PI costaining test. As shown in Figure 5h, the death rate of SKOV-3 cells induced by $Z_{\text{HER2:342}}\text{-25MFS03-PE24}$ was the highest (63.72%), compared to those induced by $Z_{\text{HER2:342}}\text{-25Cys-PE24}$ (44.40%), PE24 (19.83%), and PBS (1.80%), and the quantitative analysis result in Figure 5i indicated that the live-cell ratio in the $Z_{\text{HER2:342}}\text{-25MFS03-PE24}$ group was 1.44-fold lower than that of the $Z_{\text{HER2:342}}\text{-25Cys-PE24}$ group. Meanwhile, as shown in Figure 5j,k, the death rate of A-431 cells induced by Adnectin-17MFS01-PE24 reached 96.68%, and the live cell ratio was 19.21-fold lower than that of the Adnectin-17Cys-PE24 group. All of these results collectively demonstrated that covalent binding enhanced the cytotoxicity of affinity protein drugs *in vitro*.

Covalent Binding Improves Drug Retention and Boosts Drug Efficacy. To assess whether covalent binding could enhance the tumor accumulation of affinity protein drugs, we employed various Cy5.5-labeled conjugates to investigate drug accumulation in tumor-bearing mice via *in vivo* fluorescence imaging. As shown in Figure 6a, $Z_{\text{HER2:342}}\text{-25MFS03-PE24}$ accumulated more rapidly in the tumor, with higher uptake, compared with $Z_{\text{HER2:342}}\text{-25Cys-PE24}$, and the fluorescence intensity remained at a high level even 48 h postinjection. Furthermore, the tumor fluorescence signal–time curves of the $Z_{\text{HER2:342}}\text{-25MFS03-PE24}$ and $Z_{\text{HER2:342}}\text{-25Cys-PE24}$ groups (Figure 6b) indicated that the integrated area under the curve (AUC) of $Z_{\text{HER2:342}}\text{-25MFS03-PE24}$ was 2.19 times larger than that of $Z_{\text{HER2:342}}\text{-25Cys-PE24}$ (Figure 6c). Subsequently, the tumors and major organs of mice were further harvested for *ex vivo* analysis. As shown in Figure 6d, the fluorescence signals in the heart, spleen, lung, and kidney were qualitatively comparable between the $Z_{\text{HER2:342}}\text{-25MFS03-PE24}$ and $Z_{\text{HER2:342}}\text{-25Cys-PE24}$ groups, suggesting that the covalent modification did not appreciably alter the distribution of the drug in most normal organs. However, for the tumor site, a notable difference was observed, the quantitative analysis of tumoral fluorescence of the $Z_{\text{HER2:342}}\text{-25MFS03-PE24}$ group still exhibited that its fluorescence intensity was approximately 2.14-fold higher than that of the $Z_{\text{HER2:342}}\text{-25Cys-PE24}$ group after injection of 48 h. Meanwhile, it was remarkable that the fluorescence intensity of the liver in the $Z_{\text{HER2:342}}\text{-25MFS03-PE24}$ group was a little higher than that in the $Z_{\text{HER2:342}}\text{-25Cys-PE24}$ group, which may be attributed to the sustained release of Cy5.5 during the degradation process of high-concentration conjugates at the tumor site. All the above results confirmed that covalent binding could significantly enhance the tumor uptake and retention time of affinity protein drugs.

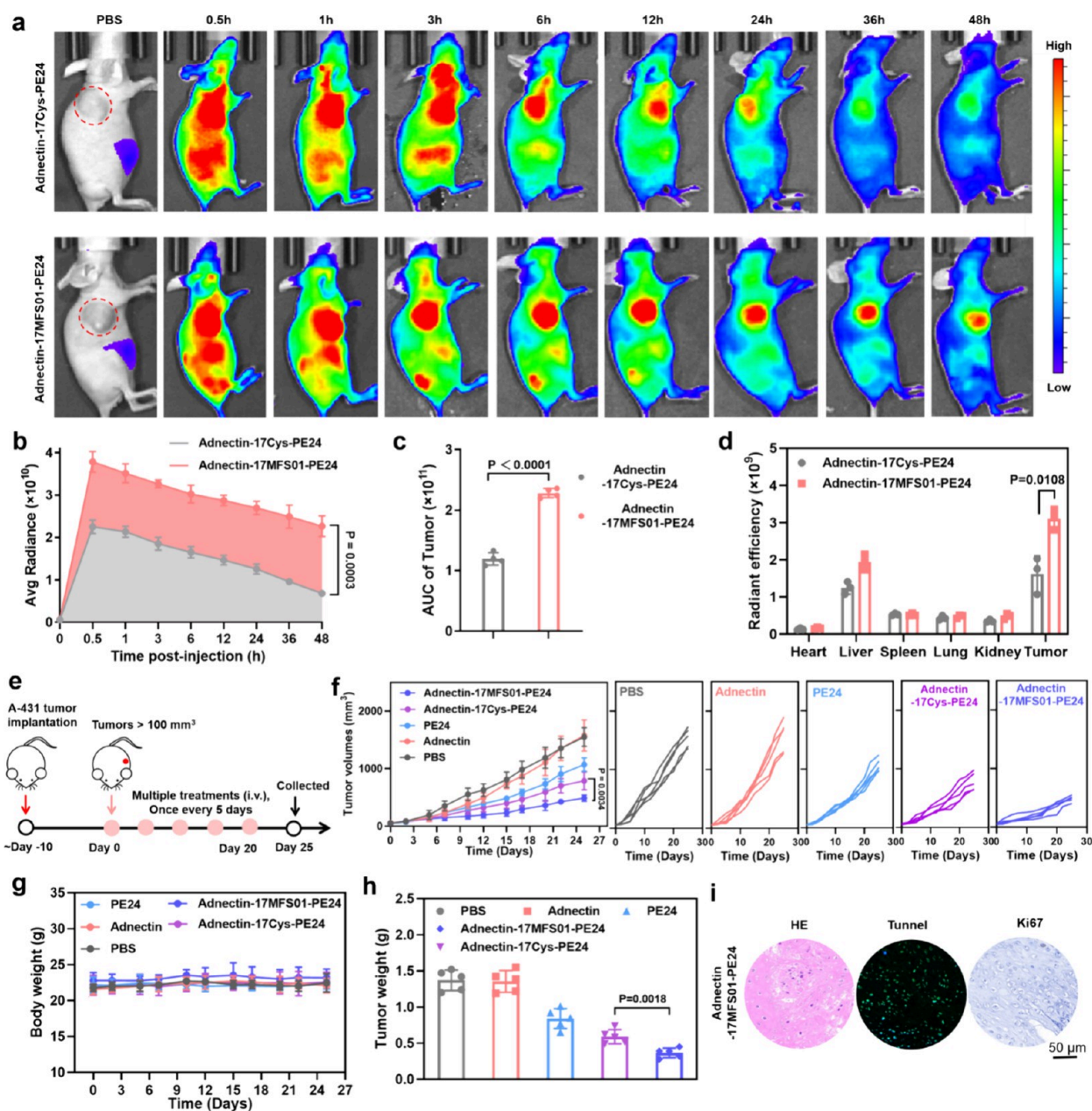


Figure 7. Improved tumor uptake and enhanced antitumor efficacy of Adnectin-17MFS01-PE24 in the EGFR overexpressed tumor model. (a) *In vivo* fluorescence imaging of the A-431 tumor model treated with Cy5.5-labeled Adnectin-17Cys-PE24 and Cy5.5-labeled Adnectin-17MFS01-PE24. The red dashed circle indicates the tumor site. (b) Time–fluorescence intensity curves of tumor sites within 48 h after administration. (c) Integrated AUC of different groups. (d) Quantitative analysis of tissue distribution in mice of different groups after injection of 48 h. (e) Schematic diagram of the antitumor experiment. (f) Tumor growth curves of each group with different treatments. (g) Body weight changes of the mice during the treatment. (h) Average weight of collected tumors at the end of experiment. (i) Histological and immunohistochemical analysis of the residual tumor in the Adnectin-17MFS01-PE24 group (the related results of other groups are exhibited in Figure S25). *P* values are determined with two-tailed unpaired Student's *t* test. Data are presented as means \pm SD from three (d, i), four (a–c), or five (f–h) independent experiments.

Furthermore, we wondered whether the increasing the tumoral retention of covalent affinity protein drugs was substantial enough to influence their antitumor effects. To address this issue, we subsequently explored the *in vivo* antitumor activity of $Z_{\text{HER2:342}}\text{-25MFS03-PE24}$ in the HER2 overexpressed SKOV-3 tumor model. Tumor-bearing mice were intravenously administered with PBS, PE24 (3 mg kg^{-1}), $Z_{\text{HER2:342}}\text{-25Cys-PE24}$, and $Z_{\text{HER2:342}}\text{-25MFS03-PE24}$ (with an equivalent dose of PE24 at 3 mg kg^{-1}) every 3 days for a total of 10 injections (Figure 6e). As shown in Figure 6f, in PBS, PE24, and $Z_{\text{HER2:342}}\text{-25Cys-PE24}$ treatment groups, the

volumes of the SKOV-3 tumors were increased more than 12.09-, 8.95-, and 6.06-fold after 30 days of treatment, respectively. However, for the $Z_{\text{HER2:342}}\text{-25MFS03-PE24}$ group, most of the tumors ceased to grow and even several ones exhibited a shrinkage in volume after the entire treatment course. Compared with that of the PBS group, the body weights of mice in the $Z_{\text{HER2:342}}\text{-25MFS03-PE24}$ group showed no discernible changes (Figure 6g), indicating the favorable biosafety property of $Z_{\text{HER2:342}}\text{-25MFS03-PE24}$. At the end of the treatment, all mice were euthanized, and their tumors were collected for *ex vivo* weighing. As shown in Figure 6h, the *ex*

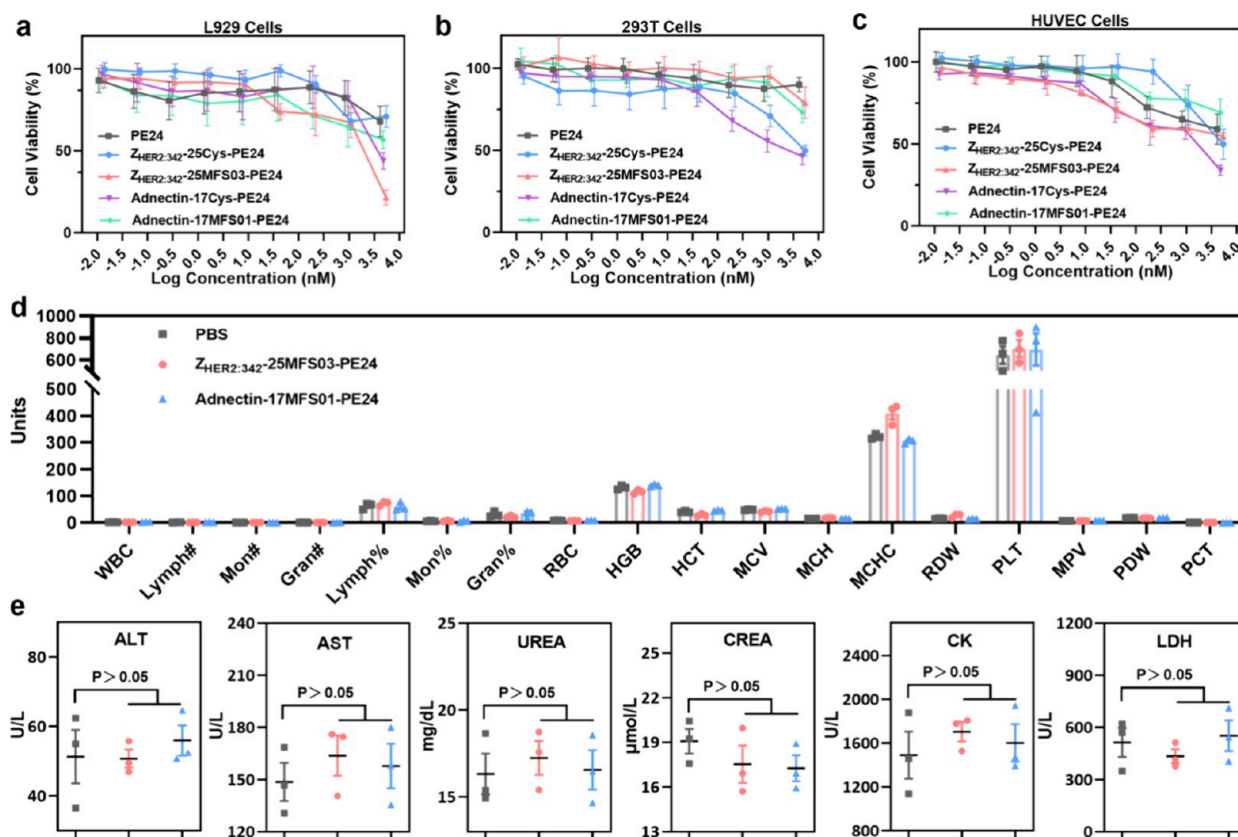


Figure 8. Good *in vitro* and *in vivo* biosafety of covalently targeted affinity protein drugs. Relative cell viability of L929 (a), 293T (b), and HUVEC (c) cells after different treatments. Hematological parameter (d) and blood biochemical (e) analyses of mice after the treatment was completed. Hematology indicators: white blood cells, WBC; lymphocyte, Lymph#; monocyte, Mon#; neutrophils, Gran#; red blood cells, RBC; hemoglobin, HGB; hematocrit, HCT; mean corpuscular volume, MCV; mean corpuscular hemoglobin, MCH; mean corpuscular hemoglobin concentration, MCHC; coefficient of variation of erythrocyte distribution width, RDW; platelet, PLT; mean platelet volume, MPV; platelet distribution width, PDW; platelet crit, PCT. Blood biochemical analysis: alanine aminotransferase, ALT; aspartate aminotransferase, AST; blood urea nitrogen, UREA; creatinine, CREA; creatine kinase, CK; lactate dehydrogenase 1, LDH. Data are presented as means \pm SD from three (d, e) or six (a–c) independent experiments.

in vivo averaged tumor weight of the $Z_{HER2:342}$ -25MFS03-PE24-treated group was approximately 0.08 ± 0.02 g; however, those of PBS-, PE24-, and $Z_{HER2:342}$ -25Cys-PE24-treated groups were about 0.98 ± 0.14 , 0.70 ± 0.10 , and 0.38 ± 0.12 g, respectively, indicating the significantly superior anticancer efficacy of $Z_{HER2:342}$ -25MFS03-PE24 compared with those of other treatment groups. Finally, histological and immunohistochemical analyses of the residual tumors were conducted. As shown in Figure 6i and Figure S24, a larger area of cell apoptosis and lower counts of positively stained cells were observed in the $Z_{HER2:342}$ -25MFS03-PE24-treated group compared with those of other treated groups, further confirming the superior antitumor activity of $Z_{HER2:342}$ -25MFS03-PE24.

As expected, covalent binding improves the drug retention and results in excellent antitumor performance in the above examples. To further validate this point, we subsequently investigated the *in vivo* antitumor property of Adnectin-17MFS01-PE24 in the EGFR overexpressed A-431 tumor model. First, we examined the drug accumulation of Adnectin-17MFS01-PE24 in A-431 tumor-bearing mice. As shown in Figure 7a, the Adnectin-17MFS01-PE24 group demonstrated the more rapid, stronger, and more persistent enrichment of drugs at the tumor site compared with that of the Adnectin-17Cys-PE24 group, and the fluorescence intensity was maintained at a rather high level 48 h postinjection. The

subsequent integrated AUC of the Adnectin-17MFS01-PE24 group was 1.91 times greater than that of the Adnectin-17Cys-PE24 group (Figure 7b,c). Moreover, as shown in Figure 7d, the results of *ex vivo* analysis for Adnectin-17MFS01-PE24 and Adnectin-17Cys-PE24 groups demonstrated comparable fluorescence signals in the major organs of mice, indicating the negligible influence of covalent modification on the drug distribution in normal organs. In contrast, significant disparity was observed at the tumor site, where the fluorescence intensity of Adnectin-17MFS01-PE24 was nearly 1.80-fold higher than that of Adnectin-17Cys-PE24. All of the above data confirmed that the covalent binding of Adnectin-17MFS01-PE24 enhanced its accumulation and retention in tumors.

Subsequently, the antitumor activity of Adnectin-17MFS01-PE24 in the A-431 tumor model was evaluated. It is noteworthy that the maximum tolerated dose of Adnectin-17MFS01-PE24 (PE24 equiv dose only at 0.1 mg kg^{-1}) in mice was significantly lower than that of $Z_{HER2:342}$ -25MFS03-PE24 (PE24 equiv dose at 3 mg kg^{-1}). The lower tolerated dose of Adnectin-17MFS01-PE24 might be due to the reported dose-limiting adverse effects of EGFR-targeting immunotoxins.^{39,40} The mice were divided into five groups and injected by the tail vein with PBS, PE24 (0.1 mg kg^{-1}), Adnectin (0.06 mg kg^{-1}), Adnectin-17Cys-PE24, and

Adnectin-17MFS01-PE24 (with an equivalent dose of PE24 at 0.1 mg kg^{-1}) once every 5 days for a total of five times (Figure 7e). The results in Figure 7f exhibited that the volumes of A431 tumors increased rapidly in PBS-, PE24-, Adnectin-, and Adnectin-17Cys-PE24-treated groups, while that in the Adnectin-17MFS01-PE24-treated group was much slower. The final collected tumor residue weight of the Adnectin-17MFS01-PE24 group was about $0.36 \pm 0.06 \text{ g}$, which was 1.61 times lighter than that of the Adnectin-17Cys-PE24 group ($0.59 \pm 0.09 \text{ g}$), further confirming the enhanced antitumor effect by covalent binding (Figure 7h). In contrast to those of other groups, the body weights of mice in the Adnectin-17MFS01-PE24 group exhibited no discernible changes (Figure 7g), suggesting the favorable biosafety of Adnectin-17MFS01-PE24. After all treatments, histological and immunohistochemical analyses of the residual tumor were conducted and are presented in Figure 7i and Figure S25. Compared with those of other groups, a larger area of cell apoptosis and a lower count of positively stained cells were observed in the Adnectin-17MFS01-PE24-treated group, effectively validating its superior antitumor activity.

Biosafety of Covalent Targeted Affinity Protein Drugs. The *in vitro* and *in vivo* biosafety is a crucial concern for drug candidates, particularly for covalent drugs; potential side effects resulting from latent off-target reactions should be paid attention.^{41,42} Here, we investigated the *in vitro* biosafety of $Z_{\text{HER2:342}}\text{-25MFS03-PE24}$ and Adnectin-17MFS01-PE24 through the CCK-8 assay. Three normal cell lines, L929 (mouse fibrosis cells), 293T (human embryonic kidney cells), and HUVEC (human umbilical vein endothelial cells), were selected to evaluate the impact of covalent binding drugs on normal cells. As shown in Figure 8a–c, the proliferation inhibitory effect on normal cells was essentially equivalent to that of the noncovalent control group at the same concentration, and the cell viability of L929, 293T, and HUVEC all remained above 60% after treatment with $Z_{\text{HER2:342}}\text{-25MFS03-PE24}$ and Adnectin-17MFS01-PE24 for 48 h at the high concentration of $10 \mu\text{M}$. These results confirmed that it was acceptable that the *in vitro* biosafety of covalent affinity protein drugs was acceptable for normal cells.

The *in vivo* biosafety of these covalent drugs was also evaluated by healthy female BALB/c nude mice. The mice were randomly divided into three groups ($n = 3$) and treated with PBS, $Z_{\text{HER2:342}}\text{-25MFS03-PE24}$ (with a PE24 equiv dose of 3 mg kg^{-1} , once every 3 days for a total of 10 times), and Adnectin-17MFS01-PE24 (with a PE24 equiv dose of 0.1 mg kg^{-1} , once every 5 days for a total of five times). After all treatments, the blood and major organs of the mice were harvested to evaluate the potential toxicity of the drugs. As shown in Figure 8d,e, in contrast to the PBS group, no discernible alterations were observed in the levels of alanine transaminase (ALT), aspartate transaminase (AST), blood urea nitrogen (UREA), creatinine (CREA), creatine kinase (CK), and lactate dehydrogenase 1 (LDH 1) for $Z_{\text{HER2:342}}\text{-25MFS03-PE24}$ and Adnectin-17MFS01-PE24 groups. Furthermore, all hematological parameters, primarily encompassing white blood cells (WBC), red blood cells (RBC), hemoglobin (HGB), and platelets (PLT), of mice treated with covalent drugs exhibited no significant differences when compared to those of the PBS group. Additionally, hematoxylin and eosin (H&E) staining of major organs also revealed no obvious pathological damage in all mouse groups (Figure S26). All these results collectively demonstrated the

negligible hepatotoxicity, nephrotoxicity, hematotoxicity, and organ toxicity of $Z_{\text{HER2:342}}\text{-25MFS03-PE24}$ and Adnectin-17MFS01-PE24, indicating the favorable *in vitro* and *in vivo* biosafety of these covalent affinity protein drugs.

CONCLUSIONS

Distinct from the reversible affinity dissociation process between traditional proteins/targets, covalent affinity protein drugs reported in this work can undergo irreversible cross-linking through the proximity-enabled reactive (PERx) between the aryl fluorosulfate in the MFS linker and the nucleophilic residue in the target, thereby forming a promising drug mode with fast tumor targeting, permanent receptor binding, effective drug accumulation, and rapid residue metabolism. Based on the covalent linkage, MSF-modified affinity protein drugs can be permanently anchored to their target proteins with a zero off-rate, thereby decoupling pharmacodynamic effects from pharmacokinetics. Leveraging this property, the MSF modification now enables the direct *in vivo* use of small affinity proteins without the need for additional half-life extension. We believe that this will facilitate their therapeutic applications in the future.

By chemical modification to attach the SuFEx-engineered MFS linker onto affinity proteins, nine HER2-targeted and nine EGFR-targeted covalent affinity protein drug candidates were facilely prepared. Subsequently, the best covalent drugs with the highest covalent cross-linking efficiency to its target were rapidly screened from these 18 candidates and characterized through additional analysis. As a proof of concept, we further demonstrated that the incorporation of the MFS linker into the HER2-specific affibody and EGFR-specific monoclonal antibody resulted in covalent targeted affinity protein drugs, which exhibited sustained and significantly enriched accumulation in tumor tissues. The accumulation was 201 and 180% higher than that of their noncovalent counterparts, respectively, and ultimately led to improved antitumor effects in the related tumor models. These findings suggest that the MFS linker can act as a versatile tool for enhancing the efficacy of targeted therapies, potentially broadening the clinical applications of affinity protein drugs. Furthermore, the direct introduction of the MFS linker into the affinity protein described in this work represents a highly convenient and efficient approach to convert classical protein drugs into covalent form, providing a general route for covalently targeting native receptors.

Because these affinity proteins were produced through traditional bacteria fermentation techniques, the covalent drug candidates guided by our strategy could be prepared in large quantities. Such advancements could pave the way for cost-effective, large-scale production of these promising therapeutic agents. This would not only streamline the manufacturing process but also lower the overall cost, making protein drugs with SuFEx latent warheads more accessible to patients in need. By integration of these innovative approaches, the pharmaceutical industry could soon unlock the full potential of these powerful therapeutic agents.

Meanwhile, it is crucial to ensure that the introduced MFS linkers do not react with intramolecular adjacent nucleophilic residues.^{14,28} This can be achieved by first analyzing the crystal structure of the target protein to determine the precise distances between potential MFS linker introduction sites and nearby nucleophilic amino acids. By identification of the optimal site for introducing an MFS linker with an appropriate

length based on this analysis, the risk of intramolecular covalent conjugation can be significantly reduced.

In this work, we choose PE24 as the active drug moiety since there is no cysteine in its original sequence.²⁷ This situation facilitates the introduction of the only cysteine into the affinity protein sequence, avoiding the chaotic coupling of MFS in the presence of multiple Cys, which is somewhat beneficial for promptly verifying the concept of our work. Moreover, for our covalent drug construction strategy, the affinity protein can not only fuse with the protein toxin but also conjugate with general small-molecule therapeutic agents such as chemical cytotoxins or radioactive drugs. The conjugation of these therapeutic agents can be readily achieved through common protein linking methods, including the Sortase A enzyme-catalyzed LPETG/GGG system, the SpyTag/SpyCatcher system, and so on.^{43–45} This versatility ensures wide applicability for our strategy, allowing for the adaptation of various therapeutic agents to combat different diseases.

Looking forward, with the rapid development of intelligent computational tools such as AlphaFold 3, the prediction of protein structures and interactions is becoming more convenient.⁴⁶ Deciding where to place the MFS linker to generate the covalent bond will be much easier, which provides broad opportunities for endowing a covalent binding ability to an immense number of proteins. We hope that this simple chemical modification strategy reported here can be further expanded to a wide range of protein molecules for further application.

■ ASSOCIATED CONTENT

SI Supporting Information

The Supporting Information is available free of charge at <https://pubs.acs.org/doi/10.1021/jacs.5c02212>.

¹H NMR and mass data for all compounds and additional experimental details, materials, methods, and figures (DOCX)

■ AUTHOR INFORMATION

Corresponding Authors

Xuelin Xia – School of Chemistry and Chemical Engineering, Frontiers Science Center for Transformative Molecules, Shanghai Jiao Tong University, Shanghai 200240, People's Republic of China; orcid.org/0009-0006-8371-0527; Email: xuelinxia@sjtu.edu.cn

Xiao-Xia Xia – State Key Laboratory of Microbial Metabolism, School of Life Sciences and Biotechnology, Shanghai Jiao Tong University, Shanghai 200240, People's Republic of China; orcid.org/0000-0001-8375-1616; Email: xiaoxiaxia@sjtu.edu.cn

Deyue Yan – School of Chemistry and Chemical Engineering, Frontiers Science Center for Transformative Molecules, Shanghai Jiao Tong University, Shanghai 200240, People's Republic of China; XIANGFU Laboratory, Jiaying, Zhejiang 314102, People's Republic of China; orcid.org/0000-0003-0969-227X; Email: dyyan@sjtu.edu.cn

Authors

Wenhui Gao – School of Chemistry and Chemical Engineering, Frontiers Science Center for Transformative Molecules, Shanghai Jiao Tong University, Shanghai 200240, People's Republic of China

Xiaoyuan Yang – School of Chemistry and Chemical Engineering, Frontiers Science Center for Transformative Molecules, Shanghai Jiao Tong University, Shanghai 200240, People's Republic of China

Wei Huang – School of Chemistry and Chemical Engineering, Frontiers Science Center for Transformative Molecules, Shanghai Jiao Tong University, Shanghai 200240, People's Republic of China; XIANGFU Laboratory, Jiaying, Zhejiang 314102, People's Republic of China; orcid.org/0000-0002-7885-4378

Complete contact information is available at: <https://pubs.acs.org/10.1021/jacs.5c02212>

Author Contributions

[‡]X.X. (Xuelin Xia) and W.G. contributed equally. The manuscript was written through contributions of all authors. All authors have given approval to the final version of the manuscript.

Notes

The authors declare no competing financial interest.

■ ACKNOWLEDGMENTS

This work was supported by the National Natural Science Foundation of China (22201178). We thank Dr. Jingli Hou and Dr. Zheng Jin from the Instrumental Analysis Center of Shanghai Jiao Tong University for technical support with tandem MS experiments. Moreover, we also thank Prof. Peng R. Chen and Postdoc Yu Han from the Beijing University for the valuable suggestion in tandem MS data analysis. The related icons used in Figure 1¹ were created in BioRender. <https://BioRender.com/k64y425>.

■ REFERENCES

- (1) Ståhl, S.; Gräslund, T.; Eriksson Karlström, A.; Frejd, F. Y.; Nygren, P.-Å.; Löfblom, J. Affibody Molecules in Biotechnological and Medical Applications. *Trends Biotechnol.* **2017**, *35* (8), 691–712.
- (2) Luo, R.; Liu, H.; Cheng, Z. Protein Scaffolds: Antibody Alternatives for Cancer Diagnosis and Therapy. *RSC Chem. Biol.* **2022**, *3* (7), 830–847.
- (3) Gebauer, M.; Skerra, A. Engineered Protein Scaffolds as Next-Generation Antibody Therapeutics. *Curr. Opin. Chem. Biol.* **2009**, *13* (3), 245–255.
- (4) Altai, M.; Liu, H.; Ding, H.; Mitran, B.; Edqvist, P.-H.; Tolmachev, V.; Orlova, A.; Gräslund, T. Affibody-Derived Drug Conjugates: Potent Cytotoxic Molecules for Treatment of Her2 over-Expressing Tumors. *J. Controlled Release* **2018**, *288*, 84–95.
- (5) Xia, X.; Yang, X.; Huang, W.; Xia, X.; Yan, D. Self-Assembled Nanomicelles of Affibody-Drug Conjugate with Excellent Therapeutic Property to Cure Ovary and Breast Cancers. *Nano-Micro Lett.* **2021**, *14* (1), 33.
- (6) Srinivasarao, M.; Galliford, C. V.; Low, P. S. Principles in the Design of Ligand-Targeted Cancer Therapeutics and Imaging Agents. *Nat. Rev. Drug Discovery* **2015**, *14* (3), 203–219.
- (7) Casi, G.; Neri, D. Antibody-Drug Conjugates and Small Molecule-Drug Conjugates: Opportunities and Challenges for the Development of Selective Anticancer Cytotoxic Agents. *J. Med. Chem.* **2015**, *58* (22), 8751–8761.
- (8) Cui, X.-Y.; Li, Z.; Kong, Z.; Liu, Y.; Meng, H.; Wen, Z.; Wang, C.; Chen, J.; Xu, M.; Li, Y.; Gao, J.; Zhu, W.; Hao, Z.; Huo, L.; Liu, S.; Yang, Z.; Liu, Z. Covalent Targeted Radioligands Potentiate Radionuclide Therapy. *Nature* **2024**, *630* (8015), 206–213.
- (9) Lai, Y.; Chu, X.; Di, L.; Gao, W.; Guo, Y.; Liu, X.; Lu, C.; Mao, J.; Shen, H.; Tang, H.; Xia, C. Q.; Zhang, L.; Ding, X. Recent Advances in the Translation of Drug Metabolism and Pharmacokinetics

netics Science for Drug Discovery and Development. *Acta Pharm. Sin. B* **2022**, *12* (6), 2751–2777.

(10) Boike, L.; Henning, N. J.; Nomura, D. K. Advances in Covalent Drug Discovery. *Nat. Rev. Drug Discovery* **2022**, *21* (12), 881–898.

(11) Péczka, N.; Orgován, Z.; Ábrányi-Balogh, P.; Keserű, G. M. Electrophilic Warheads in Covalent Drug Discovery: An Overview. *Expert Opin. Drug Discovery* **2022**, *17* (4), 413–422.

(12) Janes, M. R.; Zhang, J.; Li, L.-S.; Hansen, R.; Peters, U.; Guo, X.; Chen, Y.; Babbar, A.; Firdaus, S. J.; Darjania, L.; Feng, J.; Chen, J. H.; Li, S.; Li, S.; Long, Y. O.; Thach, C.; Liu, Y.; Zariéh, A.; Ely, T.; Kucharski, J. M.; Kessler, L. V.; Wu, T.; Yu, K.; Wang, Y.; Yao, Y.; Deng, X.; Zarrinkar, P. P.; Brehmer, D.; Dhanak, D.; Lorenzi, M. V.; Hu-Lowe, D.; Patricelli, M. P.; Ren, P.; Liu, Y. Targeting Kras Mutant Cancers with a Covalent G12c-Specific Inhibitor. *Cell* **2018**, *172* (3), 578–589.

(13) Dong, J.; Krasnova, L.; Finn, M. G.; Sharpless, K. B. Sulfur(VI) Fluoride Exchange (Sufex): Another Good Reaction for Click Chemistry. *Angew. Chem., Int. Ed.* **2014**, *53* (36), 9430–9448.

(14) Wang, N.; Yang, B.; Fu, C.; Zhu, H.; Zheng, F.; Kobayashi, T.; Liu, J.; Li, S.; Ma, C.; Wang, P. G.; Wang, Q.; Wang, L. Genetically Encoding Fluorosulfate-L-Tyrosine to React with Lysine, Histidine, and Tyrosine via Sufex in Proteins in Vivo. *J. Am. Chem. Soc.* **2018**, *140* (15), 4995–4999.

(15) Mortenson, D. E.; Brighty, G. J.; Plate, L.; Bare, G.; Chen, W.; Li, S.; Wang, H.; Cravatt, B. F.; Forli, S.; Powers, E. T.; Sharpless, K. B.; Wilson, I. A.; Kelly, J. W. “Inverse Drug Discovery” Strategy to Identify Proteins That Are Targeted by Latent Electrophiles as Exemplified by Aryl Fluorosulfates. *J. Am. Chem. Soc.* **2018**, *140* (1), 200–210.

(16) Chen, W.; Dong, J.; Plate, L.; Mortenson, D. E.; Brighty, G. J.; Li, S.; Liu, Y.; Galmozzi, A.; Lee, P. S.; Hulce, J. J.; Cravatt, B. F.; Saez, E.; Powers, E. T.; Wilson, I. A.; Sharpless, K. B.; Kelly, J. W. Arylfluorosulfates Inactivate Intracellular Lipid Binding Protein(S) through Chemoselective Sufex Reaction with a Binding Site Tyr Residue. *J. Am. Chem. Soc.* **2016**, *138* (23), 7353–7364.

(17) Li, Q.; Chen, Q.; Klauser, P. C.; Li, M.; Zheng, F.; Wang, N.; Li, X.; Zhang, Q.; Fu, X.; Wang, Q.; Xu, Y.; Wang, L. Developing Covalent Protein Drugs Via Proximity-Enabled Reactive Therapeutics. *Cell* **2020**, *182* (1), 85–97.

(18) Yu, B.; Li, S.; Tabata, T.; Wang, N.; Cao, L.; Kumar, G. R.; Sun, W.; Liu, J.; Ott, M.; Wang, L. Accelerating Perx Reaction Enables Covalent Nanobodies for Potent Neutralization of Sars-Cov-2 and Variants. *Chem.* **2022**, *8* (10), 2766–2783.

(19) Zhang, H.; Han, Y.; Yang, Y.; Lin, F.; Li, K.; Kong, L.; Liu, H.; Dang, Y.; Lin, J.; Chen, P. R. Covalently Engineered Nanobody Chimeras for Targeted Membrane Protein Degradation. *J. Am. Chem. Soc.* **2021**, *143* (40), 16377–16382.

(20) Li, S.; Wang, N.; Yu, B.; Sun, W.; Wang, L. Genetically Encoded Chemical Crosslinking of Carbohydrate. *Nat. Chem.* **2023**, *15* (1), 33–42.

(21) Sun, W.; Wang, N.; Liu, H.; Yu, B.; Jin, L.; Ren, X.; Shen, Y.; Wang, L. Genetically Encoded Chemical Crosslinking of Rna in Vivo. *Nat. Chem.* **2023**, *15* (1), 21–32.

(22) Xiang, Z.; Ren, H.; Hu, Y. S.; Coin, I.; Wei, J.; Cang, H.; Wang, L. Adding an Unnatural Covalent Bond to Proteins through Proximity-Enhanced Bioreactivity. *Nat. Methods* **2013**, *10* (9), 885–888.

(23) Wang, L.; Brock, A.; Herberich, B.; Schultz, P. G. Expanding the Genetic Code of Escherichia Coli. *Science* **2001**, *292* (5516), 498–500.

(24) Wang, L. Engineering the Genetic Code in Cells and Animals: Biological Considerations and Impacts. *Acc. Chem. Res.* **2017**, *50* (11), 2767–2775.

(25) Eigenbrot, C.; Ultsch, M.; Dubnovitsky, A.; Abrahamsén, L.; Härd, T. Structural Basis for High-Affinity Her2 Receptor Binding by an Engineered Protein. *Proc. Natl. Acad. Sci.* **2010**, *107* (34), 15039–15044.

(26) Ramamurthy, V.; Krystek, S. R.; Bush, A.; Wei, A.; Emanuel, S. L.; Das Gupta, R.; Janjua, A.; Cheng, L.; Murdock, M.; Abramczyk, B.;

Cohen, D.; Lin, Z.; Morin, P.; Davis, J. H.; Dabritz, M.; McLaughlin, D. C.; Russo, K. A.; Chao, G.; Wright, M. C.; Jenny, V. A.; Engle, L. J.; Furfine, E.; Sheriff, S. Structures of Adnectin/Protein Complexes Reveal an Expanded Binding Footprint. *Structure* **2012**, *20* (2), 259–269.

(27) Kaplan, G.; Mazor, R.; Lee, F.; Jang, Y.; Leshem, Y.; Pastan, I. Improving the in Vivo Efficacy of an Anti-Tac (Cd25) Immunotoxin by Pseudomonas Exotoxin a Domain Ii Engineering. *Mol. Cancer Ther.* **2018**, *17* (7), 1486–1493.

(28) Liu, J.; Cao, L.; Klauser, P. C.; Cheng, R.; Berdan, V. Y.; Sun, W.; Wang, N.; Ghelichkhani, F.; Yu, B.; Rozovsky, S.; Wang, L. A Genetically Encoded Fluorosulfonyloxybenzoyl-L-Lysine for Expansive Covalent Bonding of Proteins Via Sufex Chemistry. *J. Am. Chem. Soc.* **2021**, *143* (27), 10341–10351.

(29) Cao, L.; Wang, L. New Covalent Bonding Ability for Proteins. *Protein Sci.* **2022**, *31* (2), 312–322.

(30) Zhou, H.; Mukherjee, P.; Liu, R.; Evrard, E.; Wang, D.; Humphrey, J. M.; Butler, T. W.; Hoth, L. R.; Sperry, J. B.; Sakata, S. K.; Helal, C. J.; am Ende, C. W. Introduction of a Crystalline, Shelf-Stable Reagent for the Synthesis of Sulfur(VI) Fluorides. *Org. Lett.* **2018**, *20* (3), 812–815.

(31) Chen, Z.-L.; Meng, J.-M.; Cao, Y.; Yin, J.-L.; Fang, R.-Q.; Fan, S.-B.; Liu, C.; Zeng, W.-F.; Ding, Y.-H.; Tan, D.; Wu, L.; Zhou, W.-J.; Chi, H.; Sun, R.-X.; Dong, M.-Q.; He, S.-M. A High-Speed Search Engine Plink 2 with Systematic Evaluation for Proteome-Scale Identification of Cross-Linked Peptides. *Nat. Commun.* **2019**, *10* (1), 3404.

(32) Yang, B.; Wu, Y.-J.; Zhu, M.; Fan, S.-B.; Lin, J.; Zhang, K.; Li, S.; Chi, H.; Li, Y.-X.; Chen, H.-F.; Luo, S.-K.; Ding, Y.-H.; Wang, L.-H.; Hao, Z.; Xiu, L.-Y.; Chen, S.; Ye, K.; He, S.-M.; Dong, M.-Q. Identification of Cross-Linked Peptides from Complex Samples. *Nat. Methods* **2012**, *9* (9), 904–906.

(33) Li, Q.; Yang, X.; Zhao, M.; Xia, X.; Gao, W.; Huang, W.; Xia, X.; Yan, D. A Self-Assembled Affibody-Protac Conjugate Nanomedicine for Targeted Cancer Therapy. *Nano Res.* **2024**, *17* (11), 9954–9964.

(34) Klauser, P. C.; Chopra, S.; Cao, L.; Bobba, K. N.; Yu, B.; Seo, Y.; Chan, E.; Flavell, R. R.; Evans, M. J.; Wang, L. Covalent Proteins as Targeted Radionuclide Therapies Enhance Antitumor Effects. *ACS Cent. Sci.* **2023**, *9* (6), 1241–1251.

(35) Gao, W.; Yang, X.; Li, Q.; Liu, Y.; Huang, W.; Xia, X.; Yan, D. Covalent Affibody-Molecular Glue Drug Conjugate Nanoagent for Proximity-Enabled Reactive Therapeutics. *Adv. Sci.* **2025**, *12*, No. 2412273.

(36) Gao, W.; Xia, X.; Yang, X.; Li, Q.; Xia, X.; Huang, W.; Yan, D. Amphiphilic Affibody-Protac Conjugate Self-Assembled Nanoagents for Targeted Cancer Therapy. *Chem. Eng. J.* **2024**, *495*, No. 153437.

(37) Weldon, J. E.; Xiang, L.; Chertov, O.; Margulies, I.; Kreitman, R. J.; FitzGerald, D. J.; Pastan, I. A Protease-Resistant Immunotoxin against Cd22 with Greatly Increased Activity against Cll and Diminished Animal Toxicity. *Blood* **2009**, *113* (16), 3792–3800.

(38) Jun, S.-Y.; Kim, D.-S.; Kim, Y.-S. Expanding the Therapeutic Window of Egfr-Targeted Pe24 Immunotoxin for Egfr-Overexpressing Cancers by Tailoring the Egfr Binding Affinity. *Int. J. Mol. Sci.* **2022**, *23*, 15820.

(39) Chaudhary, V. K.; FitzGerald, D. J.; Adhya, S.; Pastan, I. Activity of a Recombinant Fusion Protein between Transforming Growth Factor Type Alpha and Pseudomonas Toxin. *Proc. Natl. Acad. Sci. U. S. A.* **1987**, *84* (13), 4538–4542.

(40) Niesen, J.; Stein, C.; Brehm, H.; Hehmann-Titt, G.; Fendel, R.; Melmer, G.; Fischer, R.; Barth, S. Novel Egfr-Specific Immunotoxins Based on Panitumumab and Cetuximab Show in Vitro and Ex Vivo Activity against Different Tumor Entities. *J. Cancer Res. Clin. Oncol.* **2015**, *141*, 2079–2095.

(41) Wang, Q.; Sun, T.; Xu, J.; Shen, Z.; Briggs, S. P.; Zhou, D.; Wang, L. Response and Adaptation of Escherichia Coli to Suppression of the Amber Stop Codon. *ChemBioChem.* **2014**, *15* (12), 1744–1749.

(42) Ling, J.; O'Donoghue, P.; Söll, D. Genetic Code Flexibility in Microorganisms: Novel Mechanisms and Impact on Physiology. *Nat. Rev. Microbiol.* **2015**, *13* (11), 707–721.

(43) Theile, C. S.; Witte, M. D.; Blom, A. E. M.; Kundrat, L.; Ploegh, H. L.; Guimaraes, C. P. Site-Specific N-Terminal Labeling of Proteins Using Sortase-Mediated Reactions. *Nat. Protoc.* **2013**, *8* (9), 1800–1807.

(44) Lu, J.; Wang, H.; Tian, Z.; Hou, Y.; Lu, H. Cryopolymerization of 1,2-Dithiolanes for the Facile and Reversible Grafting-from Synthesis of Protein-Polydisulfide Conjugates. *J. Am. Chem. Soc.* **2020**, *142* (3), 1217–1221.

(45) Lee, C.; Kang, S. Development of Her2-Targeting-Ligand-Modified Albumin Nanoparticles Based on the Spytag/Spycatcher System for Photothermal Therapy. *Biomacromolecules* **2021**, *22* (6), 2649–2658.

(46) Abramson, J.; Adler, J.; Dunger, J.; Evans, R.; Green, T.; Pritzel, A.; Ronneberger, O.; Willmore, L.; Ballard, A. J.; Bambrick, J.; Bodenstein, S. W.; Evans, D. A.; Hung, C.-C.; O'Neill, M.; Reiman, D.; Tunyasuvunakool, K.; Wu, Z.; Žemgulytė, A.; Arvaniti, E.; Beattie, C.; Bertolli, O.; Bridgland, A.; Cherepanov, A.; Congreve, M.; Cowen-Rivers, A. I.; Cowie, A.; Figurnov, M.; Fuchs, F. B.; Gladman, H.; Jain, R.; Khan, Y. A.; Low, C. M. R.; Perlin, K.; Potapenko, A.; Savy, P.; Singh, S.; Stecula, A.; Thillaisundaram, A.; Tong, C.; Yakneen, S.; Zhong, E. D.; Zielinski, M.; Židek, A.; Bapst, V.; Kohli, P.; Jaderberg, M.; Hassabis, D.; Jumper, J. M. Accurate Structure Prediction of Biomolecular Interactions with AlphaFold 3. *Nature* **2024**, *630* (8016), 493–500.